A PROGNOSTICS AND HEALTH MANAGEMENT APPROACH FOR AIRCRAFT CONTROL SURFACE FREE-PLAY

Michael J. Scott[1]*, Michael J. Candon[1], Wim J.C. Verhagen[1], Oleg Levinski[2] and Pier Marzocca[1]

[1] Sir Lawrence Wackett Defence and Aerospace Centre, RMIT University, Melbourne, Victoria, Australia
[2] Defence Science and Technology Group, Fishermans Bend, Victoria, Australia
* michael.scott@rmit.edu.au

Abstract: This paper describes the numerical development of a synthetic dataset and prognostics approach for aircraft control surface free-play degradation. The significance of this research is in generating a reproducible time-series dataset of free-play growth in a trailing edge control surface that is representative of actual in-flight regimes and aircraft mission profiles. Control surface free-play requires labour-intensive maintenance, limits aircraft performance and can induce aeroelastic asymmetries, which reduces component and structure fatigue life and is costly to operators. The purpose of this work is to address the research question relating to the prediction of free-play degradation and estimation of Remaining Useful Life (RUL) using prognostics from on-board signal responses with some spatial distance from the discrete source, which in this case is wing tip displacements. The research method involves the generation of synthetic data from a modified AGARD 445.6 wing with leading-edge (LE) and trailing-edge (TE) control surfaces. The TE control surface was subjected to free-play degradation over thirty flight segments of 120 seconds duration until it reaches an approximate threshold of 0.57 degrees of movement. The predicted RUL results show that the exponential degradation model is in good agreement along the piece-wise linear actual RUL, with an overall root-mean-square-error (RMSE) value of 7.05 samples. However, the most critical stage for aircraft operations is near the nominal free-play failure threshold, which has an RMSE of 1.31 samples. The proposed numerical model developed to test Prognostics and Health Management (PHM) approaches for free-play RUL estimation will support future work with reduced signal response fidelity and added free-play sources with greater spatial distance from the sensor to source.

Keywords: Aircraft Predictive Maintenance, Degradation, Free-play, RUL, PHM.

INTRODUCTION

The work detailed in this paper aims to achieve a sound understanding of free-play degradation from the perspective of prognostics and health management (PHM) and hence advance the analysis of on-board signal responses that are generated in-flight. The successful deployment of a free-play PHM framework aims to improve aircraft performance, handling dynamics in air combat and turbulence penetration, component and airframe fatigue life, reliability, and maintainability of aircraft control

surfaces. For aircraft handling qualities, a small amount of free-play may be desirable, helping prevent over-sensitivity to unintended control motions, however, in high-demand times such as air combat, free-play can contribute to over-control, loss of accuracy and rapid pilot fatigue. It should be noted that there is no set value for this handling quality, although there is a ten percent force allowance for control adjustments to keep within the threshold of pilot perception [1]. However, for autonomous systems, the control laws used in the autopilot might become deficient and would need to adapt for free-play degradation. Moreover, the impact of control surface free-play should not be underestimated, including the introduction of unexpected limit cycle oscillations (LCO) that can significantly impact structural fatigue and may lead to flutter [2]. Hence, the motivation to develop a PHM approach is to facilitate condition-based maintenance, which can be carried out efficiently prior to nominal failure thresholds, and in extreme circumstances, can prevent catastrophic failure of components or structures in-flight.

To advance prior work on PHM for control surface free-play [3], a numerical model is proposed to assess the influencing factors that impact overall free-play degradation. This is done in a controlled environment, using flight regimes that include severe aerodynamic loading. The mission profiles are designed and sequenced to reach a nominal limit of free-play and draw on previous studies, such as research conducted on tactical aircraft flight control systems [4] and subject matter expertise. Fighter and attack aircraft accrue more airframe fatigue damaging flight hours compared to a bomber, cargo, and passenger aircraft, as a measure of accelerometer normal loads with respect to cumulative occurrences per 1,000 flight hours. Interestingly, flight demonstration aircraft (e.g., Royal Australian Air Force Roulettes performing air displays) accrue the most airframe damage [5]. Therefore, the numerical case uses Generic Fighter Aircraft (GFA) flight profiles as a basis.

Recent research work developing model-based PHM approaches and specifically on component systems such as electro-mechanical actuators (EMA), shows promising results for free-play at large magnitudes and in aged actuators, but further work is needed for smaller free-play values [6], [7]. Since existing approaches are tested on smaller datasets of limited flight profile variation [8], this paper aims to expand the test datasets through varying flight regimes and will allow testing of the PHM approaches with a widely varying set of manoeuvre conditions. This work builds on diagnostic [9] and prognostic approaches for control surface free-play that use actuator load responses and have been developed with representative flight test data of a GFA [10], [11]. This paper aims to contextualise the influencing factors of free-play growth in representative missions and focus on the high severity aerodynamic loading flight regimes that contribute to free-play growth through wear, and in this case, are characterised by a zero-stiffness free-play "dead zone" in a hinged flap.

The scope of this paper is to detail the methodologies in developing a PHM framework for control surface free-play in a numerical case, without the servicing interventions, disturbances, and other sensitivities to 'real-world' environmental conditions, therefore developing a benchmark case. Furthermore, this work aims to contribute to developing representative flight mission profiles that are particularly significant to free-play and to test the remaining useful life (RUL) of the system. These approaches are underpinning the development of aircraft predictive maintenance and enabling proactive condition-based maintenance for enhanced aircraft utilisation, planning and less downtime [12].

The numerical approach aims to represent 'real-world' free-play degradation in an aircraft control surface system. It assumes that flight regimes that encounter greater aerodynamic loading conditions on control surfaces will impact the growth of free-play the greatest. Therefore, flight conditions of Mach number, angle-of-attack, and Velocity index influence the numerical results generated and are proportional to the labelled severity of low, moderate, and high. High-severity flight conditions have high rates of change in parameters and larger ranges. For simplicity and clarity, this approach does not include all influencing factors that can increase the growth of free-play, for example, actuator's hysteresis and saturation, deformation, and thermal loading conditions that can occur during hard and tactical manoeuvring. However, it is closely modelled on surrogate flight test data experience and domain expertise, with a focus on capturing high-severity flight conditions that could include manoeuvres like vortex buffet [4].

Overall, this paper serves to detail a prognostics approach to estimating RUL for control surface free-play addressing shortcomings in literature by i) generating reproducible synthetic datasets of free-play degradation for the purposes of building robust prognostic models; and ii) developing a range of flight profiles of low, moderate, and high severity flight conditions, representative of 'real-world' free-play degradation.

The rest of the paper is structured as follows. Firstly, the research methodology used to develop the numerical model is described. This is followed by the PHM approach for RUL estimation and by the results and discussions. Concluding remarks are presented along with future work.

RESEARCH METHODOLOGY AND BENCHMARK

This numerical case study serves as a benchmark case for the development of a reliable and robust PHM approach for control surface free-play RUL estimation; hence the generation of synthetic datasets is developed with 'real-world' flight missions in consideration. While there are constraints to the numerical model, as not all factors contributing to free-play growth are considered – see discussion in the subsequent sections – the purpose of this paper is to demonstrate that free-play degradation can be modelled for prognostics while incorporating realistic aircraft utilisation and mission profiles for the purposes of supporting maintainers in operational decision-making and sustainment. As shown in Figure 1, the fundamental steps in the PHM approach are as follows: i) data generation from the conceptual flight profiles with control surface free-play growth; ii) signal processing of wing responses for feature selection to enable RUL estimation and diagnostics; and iii) the visualisation for maintainers to make a decision for how to manage the health of the aircraft in service.

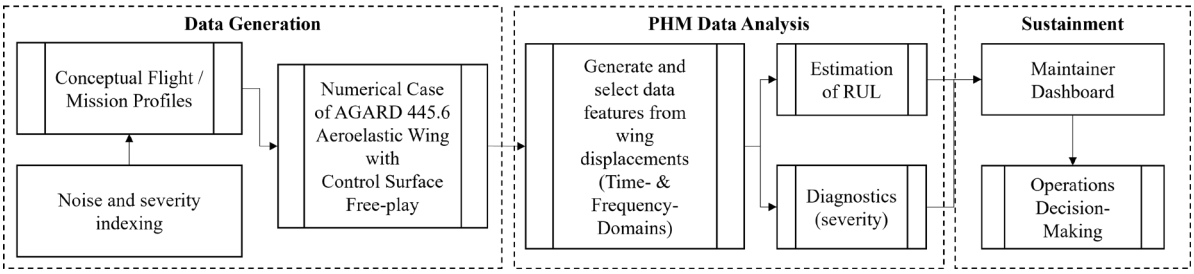

Figure 1: Flowchart of fundamental steps for the PHM numerical case study, signal processing and proposed integration for sustainment usage.

Modified AGARD 445.6 Aeroelastic Wing

The AGARD 445.6 wing model is a well-known benchmark case used to validate new aeroelastic modelling approaches for decades, with experimental data ranging from low-transonic to low-supersonic Mach numbers acquired over 30 years ago in the NASA transonic dynamic wind tunnel [13]. The wing is characterised by a weak aerodynamic non-linearity and a linear structure, resulting in typically good correlation with experiment by numerical aeroelastic frameworks [14]. For this study, the AGARD 445.6 wing tapered swept wing with a NACA 65A004 aerofoil section and sweep angle of 45° is modified to resemble a representative main wing with the LE and TE control surfaces, as presented in Figure 2. The material properties of the control surfaces are consistent of the weakened model (No. 3) from the experimental campaign. The material, geometric and mass properties of the AGARD 445.6 wing are from [15].

Computational Aeroelastic Model

A linearised state-space aeroelastic platform, including an aerodynamic reduced-order model using ANSYS MAPDL and ANSYS FLUENT, is used to capture the generalised aerodynamic forces (GAF). The 3-D wing body is modelled in modal coordinates for efficiency, which is a valid representation given the relatively small elastic displacements of the structure. To ensure that the structural variations are captured due to stiffness free-play, the affected degrees-of-freedom are loaded with large fictitious

masses (FM), which renders the structure insensitive to a local stiffness variation and is hence conveniently able to describe the total time history of the dynamic response using a single set of modes [16]. The dynamic response is captured at the LE and TE flaps and wing tips, where the TE wing tip response has a spatial distance of 0.18 metres from the TE flap with free-play. For a detailed description of the aeroelastic modelling scheme developed within the aeroelastic research group at RMIT University, see [15]; this also includes experimental and numerical validation.

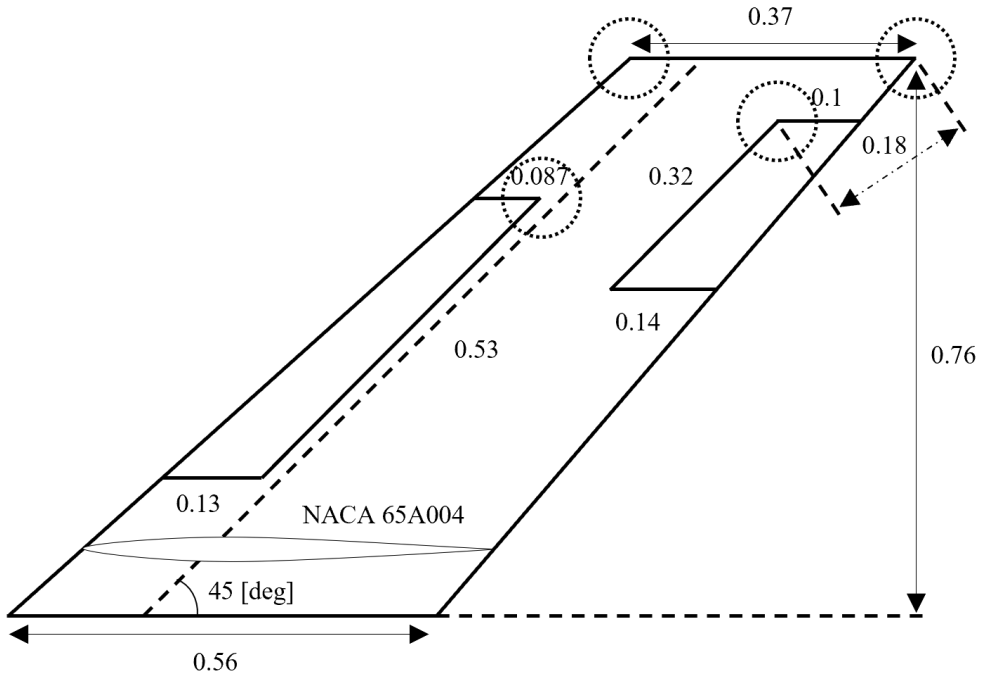

Figure 2: AGARD 445.6 swept wing model geometry specifications (measurements in metres), showing the four locations (dotted circles) where displacement responses are taken – in this case, the TE wing tip displacement is used in the PHM approach.

The control surfaces are connected to the main wing, such that their motion implicitly follows the main wing with the exception of the hinge rotation, which is controlled by a torsional stiffness of $k_{le} = k_{te} =$ 125 [Nm/rad]. The free-play magnitudes are denoted as $\delta_{s,le}$, and $\delta_{s,te}$ for the LE and TE control surface hinges, respectively. The natural frequencies (computed via the FM method) that are relevant to the free-play configurations, the control surface fixed state (nominal linear hinge stiffness) and the free state (zero hinge stiffness), considered in this paper are highlighted in Table 1. A sensitivity study was conducted, which verified that ten modes are sufficient to capture the dual-free-play behaviour. The first four mode shapes are presented in Figure 3, where bending and torsion dominated effects can be observed for the first three modes, and significant deformation of the LE control surface is observed for the fourth mode. The fifth and eighth modes are dominated by the TE control surface deflection. Mode 6 represents the second torsion mode of the LE control surface.

Table 1: Linear Modes for the modified AGARD 445.6 wing.

Mode	*TE-fixed, LE-fixed* [Hz]	*TE-free, LE-fixed* [Hz]	*TE-free, LE-free* [Hz]
ω_1	11.59	0.016	0.0104
ω_2	43.44	11.93	0.018
ω_3	51.31	42.28	12.12
ω_4	83.44	52.46	48.06
ω_5	118.41	76.23	51.85
ω_6	121.76	122.10	111.20
ω_7	130.91	130.62	130.96
ω_8	146.70	133.71	132.93
ω_9	309.82	174.39	226.18
ω_{10}	542.24	464.32	326.04

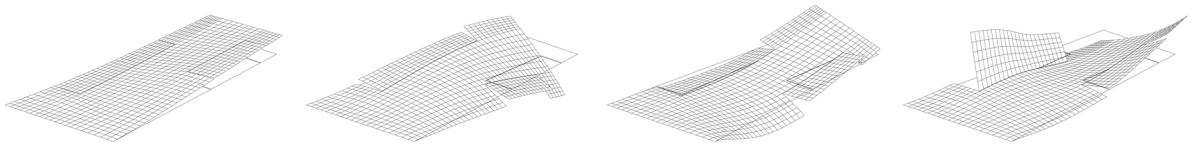

(a) *(b)* *(c)* *(d)*

Figure 3: First four natural mode shapes, *(a)* mode 1, *(b)* mode 2, *(c)* mode 3 and *(d)* mode 4.

Implementation of Dynamic Flight Parameters

Linearisation of the weakly non-linear aerodynamic forces is valid for a fixed Mach number, M_∞, and angle-of-attack, α_0. GAF must be recomputed if a change in either of these two parameters is required. Given the objective of this research, highly dynamic flight parameters are required to allow the mission profiles to be designed. This could be solved directly using a computational fluid dynamics (CFD) solver to compute the aerodynamic forces at every time-step; however, this would be computationally expensive. As a result, an interpolation scheme has been implemented whereby a GAF library is generated, and the linearised solver interpolates the GAF library according to predefined flight profiles. The GAF are computed for each permutation of M_∞ = 0.85, 0.901, 0.96, 1.072 and α_0 = 0°, 1°, 2°, 3°. Three-dimensional cubic spline interpolation is performed to extract the GAF for any combination of M and α_0 within the interpolation field, as displayed in Figure 4. The GAF are updated at every ten time-steps to improve computational efficiency, with a time step of t = 0.001s. The velocity index V^* is used to define the flight profiles, representative of the altitude and does not need to be interpolated given its validity for fixed values of M_∞ and α_0.

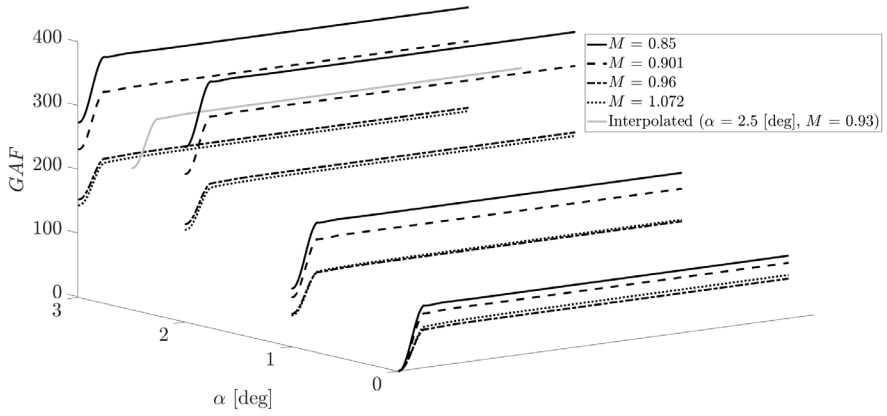

(a)

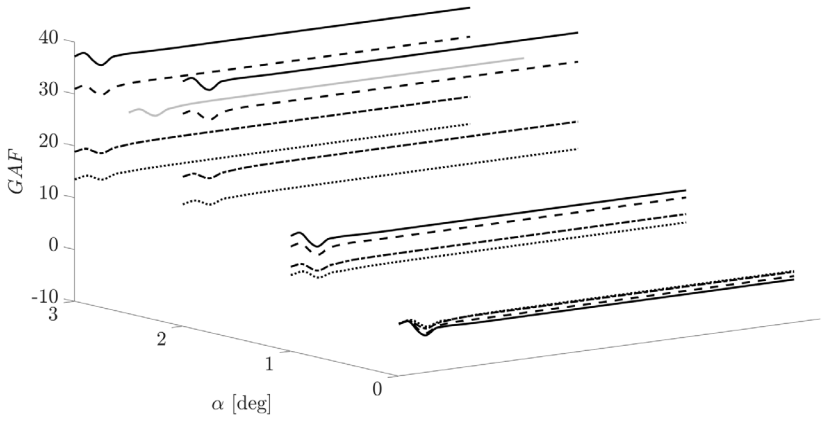

(b)

Figure 4: Example interpolation field for the GAF of *(a)* mode 1 and *(b)* mode 10.

Flight Mission Profiles

The flight profiles are developed to provide a range of conditions within MIL-SPEC 8870 requirements [17]. The mission profiles are sequenced and aligned to utilisation rates of modern GFA, for example, the Lockheed Martin F-35A Lightning II, with utilisation of approximately 250 hours, noting that this is a planned average annual flying hours per aircraft (2019 estimate), whereas in practice actual hours are lower [18]. This also reflects intervals for scheduled maintenance, which are most often flight hours driven for control surfaces. An example of this is the Pilatus PC-9 aircraft with a recommended master maintenance plan setting secondary flight control systems (e.g., flap actuator) at a flight hour check of 150 hours [19]. It should be noted that the flight profiles are constrained by the existing AGARD wing numerical model parameters and geometry, although the flight regimes, sequencing and occurrences are modelled closely to a GFA's utilisation.

The flight severity levels and sequencing are based on domain expertise knowledge and research on mission profiles of the Fairchild Republic A-10 Thunderbolt II US fleet, which analysed data from eleven years of operation [5], studying g-counts per flight hour for overall sorties consisting of varying manoeuvres. Furthermore, the manoeuvres and flight sequencing consider post-maintenance moderate severity Functional Check Flight (FCF) missions and the high severity instances being missions that include Basic Fighter Manoeuvres (BFM) or Surface Attack (SA) profiles. While lower severity flights could be Navigational Flight (NAV) missions. In Figure 5, the sequencing of these flights is represented, and the mix of missions is approximated to be 30% low, 40% moderate and 30% high severity. The range of flight parameters used to describe mission profile severity is given in Table 2.

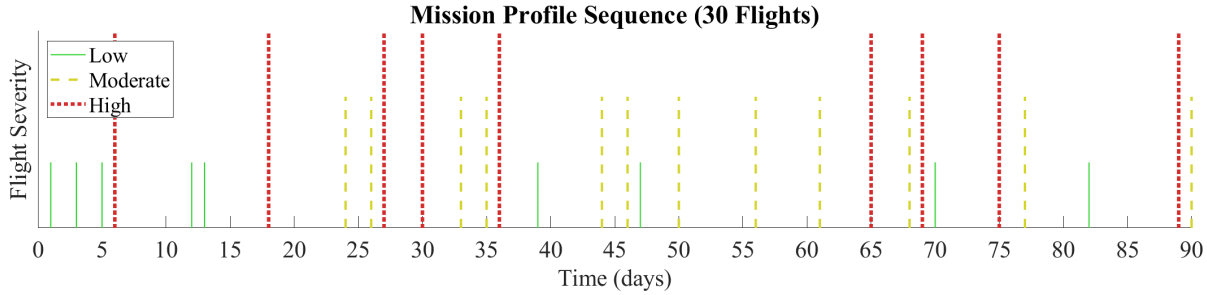

Figure 5: Example of the thirty mission profiles sequenced for the numerical case study over time with corresponding flight severity, totalling nine low, twelve moderate and nine high.

Table 2: Flight parameter ranges used to describe the mission profile severity.

Parameter [limited range]	*Low Severity*	*Moderate Severity*	*High Severity*
Mach (M_∞) [0.85 – 1.05]	0.85 – 0.9	0.85 – 0.95	0.85 – 1.05
Alpha (α_0) [0° – 3°]	0° – 1°	0° – 2°	0° – 3°
Velocity Index (V^*) [0.10 – 0.33]	0.20 – 0.33	0.15 – 0.33	0.10 – 0.33

It should be noted that within a single flight, there could be a range of manoeuvres and at different phases of flight – flight phase being a function that defines the intended use of the aircraft within a flight. Therefore, some flight phases will be more severe in aerodynamic loading and impact free-play degradation. For example, the variation of flight parameters (M_∞, α_0, V^*) takes into consideration the parameter ranges and value rate of change. Shown in Figure 6 are the representative flight phases that a typical aircraft may experience and the phases that impact the growth of free-play. The key phases are climb, manoeuvres and descent, which are marked as low, moderate, or high severity phases. The flight phases are aligned to that of a typical flight that may be in the cruise phase (or other sub-phase, such as loitering, refuelling, air-to-air tracking, low-level surface attack, etc.) for 57% of duration [20]–[24].

However, it should be noted that for a GFA, a phase of flight, like cruise, is likely to have less impact on free-play degradation compared to high speed, high rate of turn and high-alpha manoeuvres at low altitude (e.g., combat radius turn, tactical pitch, etc.), which could induce large aerodynamic loading on control surfaces caused by sustained vortex buffet flow regimes. Additionally, an important factor for

GFA is the rate of climb and the profile of altitude can be widely ranging, noting that a GFA can climb in altitude at a rate approximately fifteen times that of commercial airliners, which is typically a maximum rate of climb of around 4,000 feet per minute (~20 metres per second). For a McDonnell Douglas (now Boeing) F/A-18 Hornet aircraft, the maximum rate of climb is approximately 60,000 feet per minute (~300 metres per second) [25].

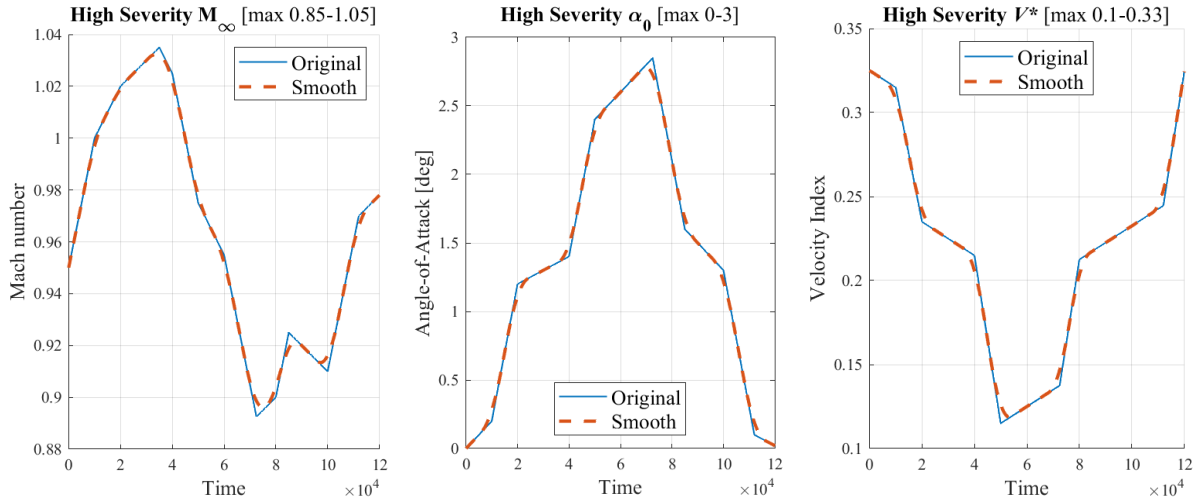

Figure 6: Example of mission profile phases of flight for flight parameters (M_∞, α_0, V^*).

The MIL-SPEC 8870 specifies that *the maximum allowable limits for a TE control surface that extends outboard of the 50 percent, but inboard of the 75 percent span station of the main surface, where the total free-play shall be not greater than 0.57° (or 0.01 radians) of movement* [17]. Therefore, the nominal failure threshold in the numerical case is set to 0.57°, which is the nearest specification for this control surface. Subsequently, the free-play initial value is set to 0.01° (0.00017 radians), under the assumption that some free-play is always in the system or is indicated due to possible measurement inaccuracies (e.g., manual static free-play tests) [26].

Free-play Degradation

The degradation of free-play is calculated as a function of the flight parameters, M_∞, α_0 and V^*, their derivatives and the current free-play (for 'wear and tear'). At every time-step, the increase in free-play is calculated, according to Eqn. 1:

$$\Delta\delta_{s,te} = (A_M {M_\infty}^{B_M} + A_\alpha {\alpha_0}^{B_\alpha} + A_V {V^*}^{B_V} + A_{\dot{M}} {\dot{M}_\infty}^{B_{\dot{M}}} + A_{\dot{\alpha}} {\dot{\alpha}_0}^{B_{\dot{\alpha}}} + A_\delta \delta_{s,te})c \quad (1)$$

where $\Delta\delta_{s,te}$ is the change in free-play for the current time-step, $\dot{M}_\infty$ and $\dot{\alpha}_0$ are the first derivatives of M_∞ and α_0 respectively, the coefficients A provide linear scaling to the flight parameter contributions, the indices B provide non-linear contributions, while c scales the entire contribution.

Figure 7 *(a)* presents the distribution of flight parameters for each of the 30 flights (as described in the previous section), where the severity of each flight can be taken from Figure 5. The significant contribution to free-play degradation is clear for the high-severity flights in Figure 7 *(b)*, which plots $\Delta\delta_{s,te}$ for each time-step, with Figure 7 *(c)* demonstrating the cumulation $\sum \Delta\delta_{s,te}$. The total free-play approaches its maximum value at the end of flight 30, at which point maintenance is required. The TE tip response (Figure 7 *(d)*) clearly demonstrates the impact of free-play on the global response of the wing, where the amplitude increases significantly as the free-play degrades.

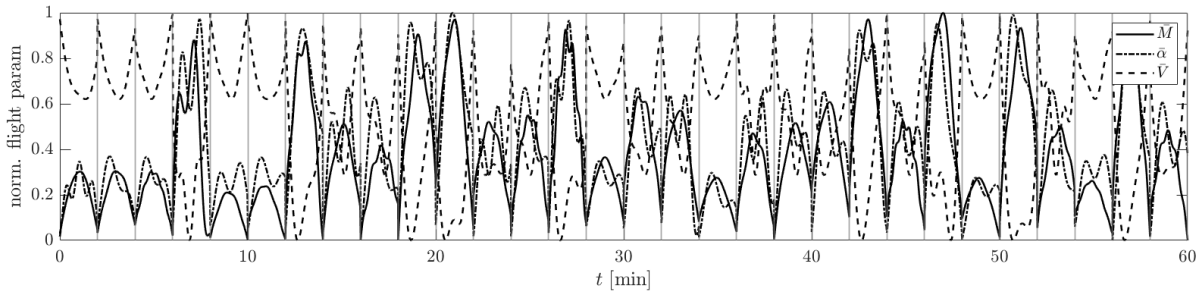

(a)

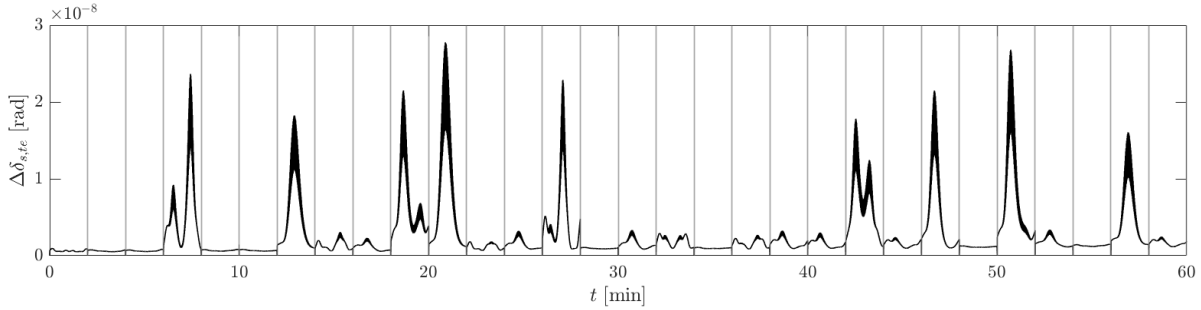

(b)

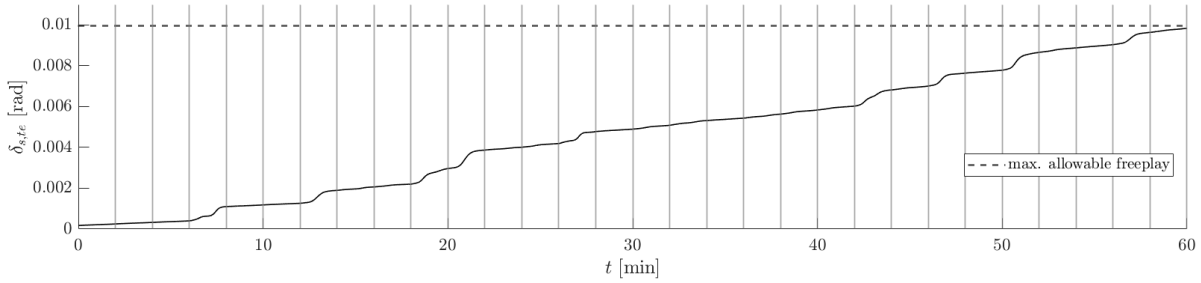

(c)

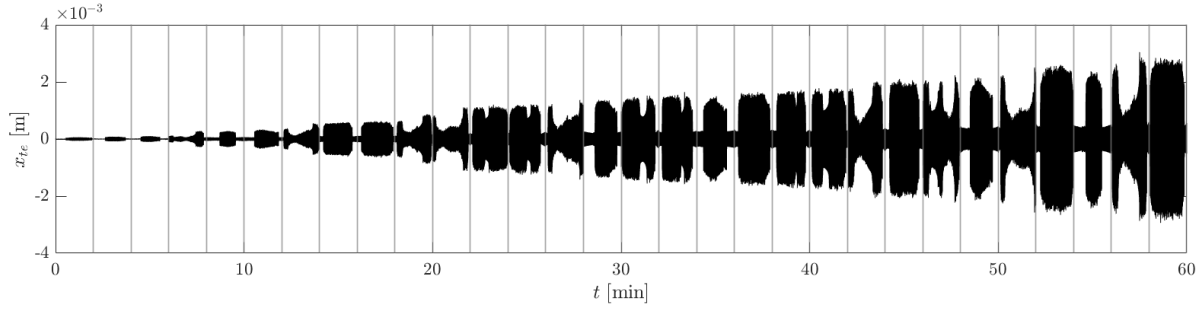

(d)

Figure 7: Results of the numerical simulation for thirty flight segments at two minutes duration with *(a)* the normalised flight parameters, *(b)* increase in free-play at each time-step, *(c)* the total free-play, and *(d)* the response of the TE tip.

Figure 8 is for consecutive flights 6, 7 and 8 that are representative of low, high, and moderate severity mission profiles, respectively. Here, the effect of the flight parameters (Figure 8 *(a)*) on the response (Figure 8 *(b)*) is clearly visible. The spectrogram (Figure 8 *(c)*) of the response in Figure 8 *(b)* is used to

verify that the frequencies in the non-linear response are valid with respect to the natural modes of the system and to provide some brief analysis. For each flight, a low-amplitude quasi-periodic response is observed initially, which is dominated by the first torsional mode, ω_3, and its harmonics $2\omega_3$, $3\omega_3$ … . The odd harmonics dominate, typical of a system with free-play non-linearity. As the flight parameters vary, there is a rapid transition to high-amplitude chaotic response, where the non-linear response is dominated by the first bending mode, ω_1, and its odd harmonics. There appear to be other non-linear frequencies acting in this chaotic response region. However, further analysis is required to better understand the non-stationary spectral behaviour which falls outside of the scope of this paper. Interestingly, the point at which an abrupt change from low-amplitude quasi-periodic to high-amplitude chaotic response is observed, there appears to be a bifurcation of the dominant mode ω_3. Similarly, when the system re-enters the low-amplitude orbit (towards the end of flights 6 and 8), the linear and non-linear modes appear to coalesce as the dominant mode ω_3 is reactivated. A paper focussing on these non-linear dynamics will be the subject of future research by the authors. Table 3 presents a detailed description of the thirty flights considered here and statistical parameters for the response data of interest.

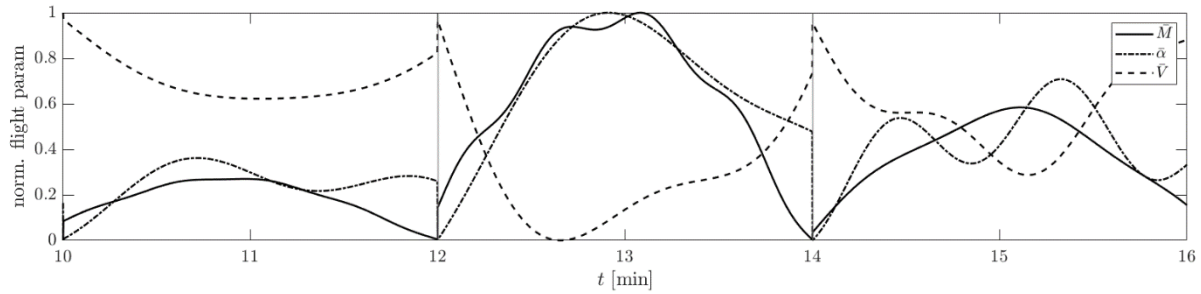

(a)

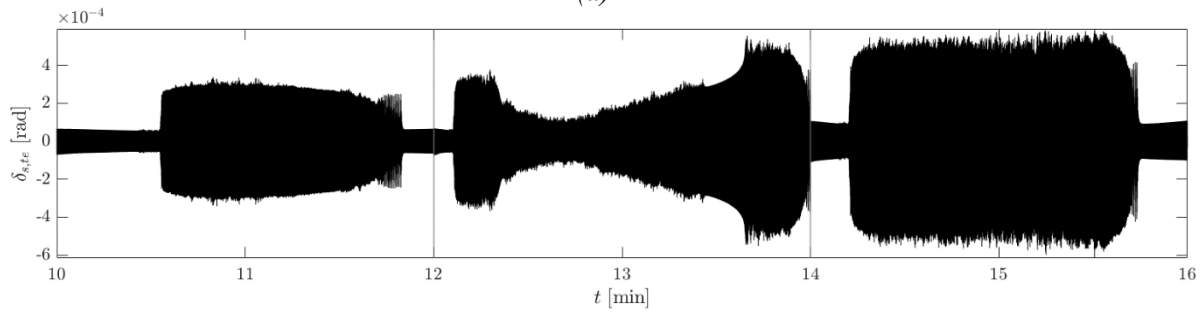

(b)

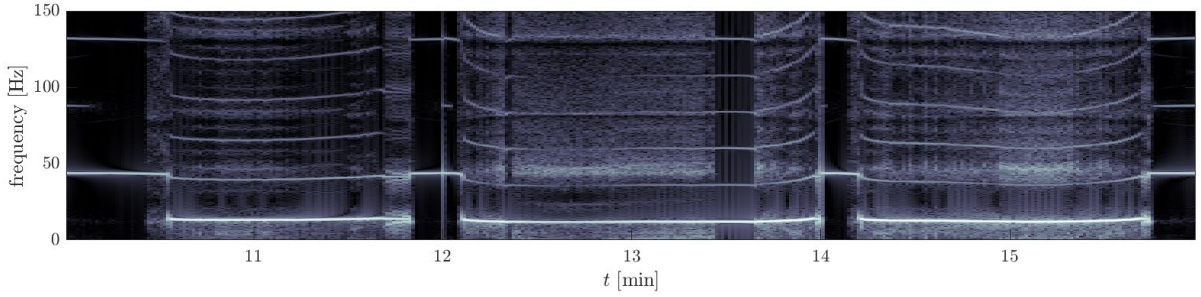

(c)

Figure 8: Results of the numerical simulation for flights 6-8 with *(a)* the normalised flight parameters, *(b)* the response of the TE tip and *(c)* the time-frequency domain representation of *(b)*.

Table 3: Numerical case study flight data analysis using the TE wing tip response (displacements) for thirty flights.

Flight #	*Date*	*Severity*	*Free-play (degrees) [start 0.01]*	*Peak Frequency (PeakFreq1)*	*Peak-to-Peak (Peak2Peak)*	*Standard Deviation (Std)*	*Root Mean Square (RMS)*	*Health Indicator*
1	01/Jan	Low	0.014435	1.306471	0.000123	2.89E-05	2.89E-05	0.000000
2	03/Jan	Low	0.018700	1.306471	0.000164	3.52E-05	3.52E-05	0.028574
3	05/Jan	Low	0.023104	1.306471	0.000203	4.12E-05	4.12E-05	0.056392
4	06/Jan	High	0.063060	1.221001	0.000560	9.34E-05	9.34E-05	0.191605
5	12/Jan	Low	0.067780	1.343101	0.000564	0.000112	0.000112	0.365602
6	13/Jan	Low	0.072408	1.330891	0.000680	0.000149	0.000149	0.591096
7	18/Jan	High	0.108625	1.208791	0.001107	0.000193	0.000193	0.924156
8	24/Jan	Mod	0.118261	1.245421	0.001207	0.000300	0.000300	1.291191
9	26/Jan	Mod	0.126150	1.245421	0.001285	0.000332	0.000332	1.687394
10	27/Jan	High	0.170045	1.221001	0.001741	0.000334	0.000334	2.088353
11	30/Jan	High	0.221666	1.208791	0.002232	0.000360	0.000360	2.474655
12	02/Feb	Mod	0.229729	1.208791	0.002389	0.000635	0.000635	3.090290
13	04/Feb	Mod	0.240037	1.233211	0.002464	0.000618	0.000618	3.640729
14	05/Feb	High	0.273840	1.208791	0.002783	0.000509	0.000509	4.024391
15	08/Feb	Low	0.280428	1.294261	0.002723	0.000607	0.000607	4.421656
16	13/Feb	Mod	0.291288	1.221001	0.003074	0.000766	0.000766	4.694746
17	15/Feb	Mod	0.304528	1.233211	0.003224	0.000792	0.000792	5.036376
18	16/Feb	Low	0.311294	1.318681	0.002997	0.000642	0.000642	5.242392
19	19/Feb	Mod	0.322540	1.282051	0.003281	0.000870	0.000870	5.670127
20	25/Feb	Mod	0.334181	1.245421	0.003439	0.000875	0.000875	5.867336
21	01/Mar	Mod	0.345104	1.221001	0.003605	0.000929	0.000929	6.103916
22	05/Mar	High	0.390401	1.221001	0.004082	0.000823	0.000823	6.502305
23	08/Mar	Mod	0.401366	1.233211	0.004169	0.001064	0.001064	6.889605
24	09/Mar	High	0.437660	1.208791	0.004462	0.000901	0.000901	7.074923
25	10/Mar	Low	0.445642	1.318681	0.004295	0.000911	0.000911	7.152172
26	15/Mar	High	0.496055	1.196581	0.005075	0.000791	0.000791	7.255941
27	17/Mar	Mod	0.508475	1.245421	0.005252	0.001410	0.001410	7.870867
28	22/Mar	Low	0.517535	1.318681	0.004804	0.000926	0.000926	7.953934
29	29/Mar	High	0.551899	1.221001	0.005908	0.001124	0.001124	8.471773
30	30/Mar	Mod	0.570000	1.221001	0.005777	0.001561	0.001561	9.589647

PHM APPROACH FOR RUL ESTIMATION AND RESULTS

The PHM approach for RUL estimation of free-play is determined by the signal response features monotonic relationship and the damage accumulation exponential degradation model parameters. The prognostics model chosen is an exponential degradation model, as the control surface free-play experiences a cumulative degradation over time [27]. The trailing-edge wing tip response undergoes feature generation, which involves analysis of the signal, sampled at 100 Hz, in time- and frequency-domain to identify suitable features for prognostics.

The 30 test points are first smoothed using a moving average over three days to capture the longer-term monotonic trend and reduce the influence of noise between test-points. A 50% / 50% split of data for training and testing purposes is performed, which results in the first 15 flights used to train the model and later test the model for accuracy. To show that diagnostics of the signal is possible, a supervised machine learning classification model is trained and tested to identify when free-play is either low in magnitude or high based on the current response. The signal features selected for diagnostics are the peak-to-peak (Peak2Peak) and peak frequency, which, when applied to a supervised linear Support Vector Machine (SVM) model, produces an overall accuracy of 93.3%, used with a k-fold cross-validation scheme (using five folds) to limit any over-fitting (see Figure 9).

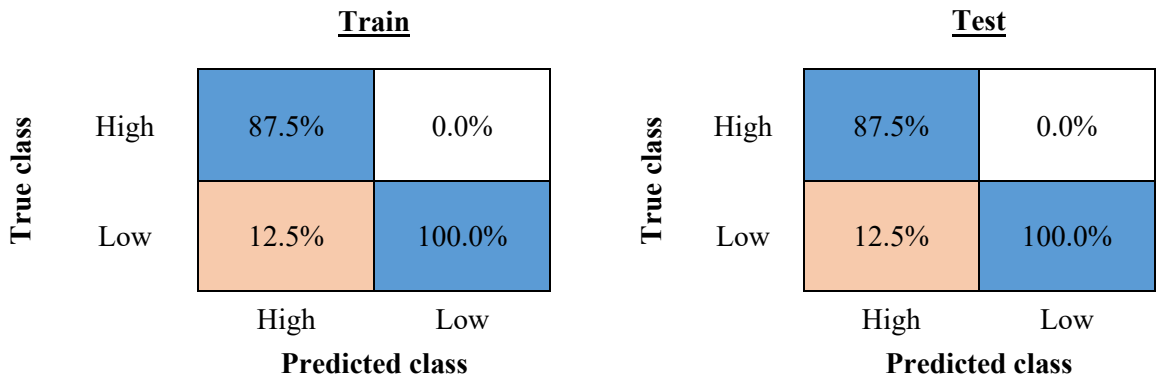

Figure 9: Free-play diagnostics results for linear SVM model - confusion chart for Train and Test classification model using only Peak2Peak and peak frequency features.

For the prognostics degradation model, the Peak2Peak is a significant feature, where the amplitude range of the signal is calculated to a value summing the absolute maximum and absolute minimum of the signal response; this can increase as system components age and degrade. To determine the health indicator for use in the degradation model, monotonicity is calculated to quantify the trend quality of a data feature. As shown in Figure 10, the highest value is 0.86 for the Peak-to-Peak feature, followed by the standard deviation (Std) and root-mean-square (RMS) at 0.71 – noting that monotonicity ranges between zero and one, where one is considered a perfect monotonic relationship and suitable for trending. The top three monotonic features are dimensionally reduced in subsequent principal component analysis (PCA) to generate a coherent and smooth health indicator.

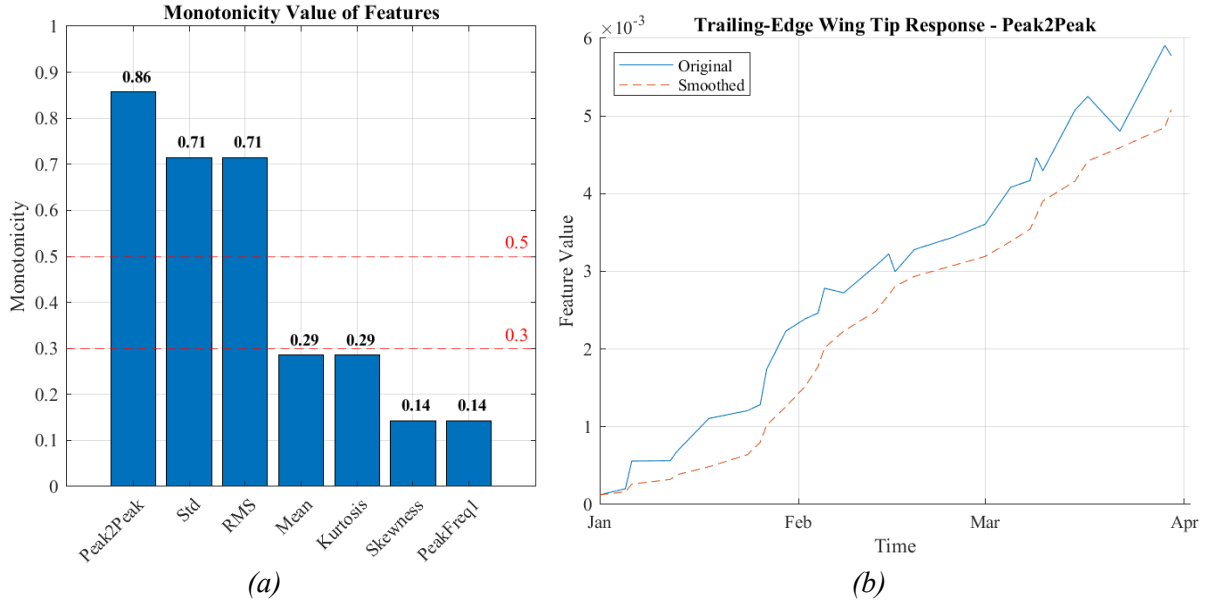

Figure 10: *(a)* Monotonicity values for signal features, where a higher value means the relationship is monotonic and useful as a health indicator; and *(b)* shows the smoothed Peak2Peak of the signal, which is the selected feature for prognostics.

There are two commonly used prognostic metrics to evaluate the performance of RUL estimations: i) RMSE as Eqn. 2; and ii) the Scoring Function as Eqn. 3, which is used in several studies as benchmarks, initially used in the PHM Challenge in 2008 [28]. The two metrics RMSE and the Scoring function, are as follows:

$$RMSE = \sqrt{\frac{1}{N}\sum_{i=1}^{N}(\hat{r}_i - r_i)^2} \tag{2}$$

$$Score = \begin{cases} \sum_{i=1}^{N}\left(e^{-\left(\frac{\hat{r}_i - r_i}{13}\right)} - 1\right), & \text{for } \hat{r}_i < r_i \\ \sum_{i=1}^{N}\left(e^{\left(\frac{\hat{r}_i - r_i}{10}\right)} - 1\right), & \text{for } \hat{r}_i \geq r_i \end{cases} \tag{3}$$

where N is the number of measurements, while $\hat{r}_i$ is the estimated RUL, and r_i is the observed actual RUL. It should be noted that the best value for both metrics is zero. The RMSE metric is useful for general comparison purposes; however, it is a symmetric loss value and quantifies the same error penalty for over- and under-predictions. It is important to note that RUL predictions that are over-estimated can have greater consequences in practice than under-estimating the RUL of a component or system (i.e., component failures in-service before being maintained as the prediction is over-estimated, as opposed to being maintained early). Therefore, the scoring function is used, which penalises over-estimated predictions of RUL [29], [30]; although these metrics may not align with operational considerations for end-users.

Figure 11 shows the results for the prognostics approach, where the alpha (α) – lambda (λ) performance plot is used as a metric for RUL as it accounts for prediction accuracy at specific time instances; for example, alpha is set to 20% after a fault detection, allowing for margin in RUL from the relative distance (lambda) to actual failure [31]. This then correlates to the probability of predicted RUL within the alpha bound, giving a probabilistic value at each time instance for the accuracy of RUL estimation.

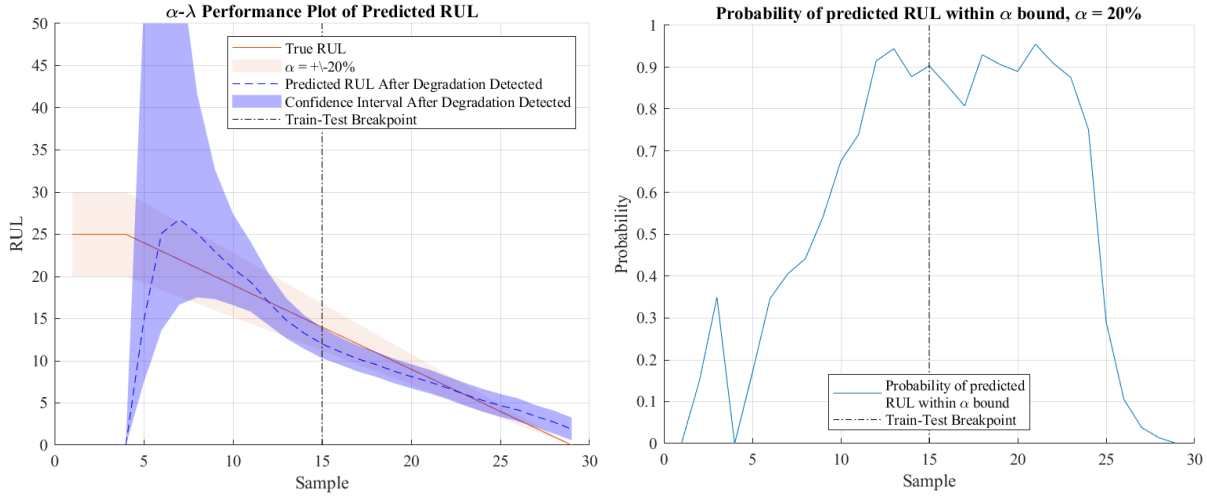

(a) *(b)*

Figure 11: *(a)* alpha-lambda performance plot showing predicted RUL and true RUL; and *(b)* the probability of predicted RUL accuracy within the alpha bound of 20% of the true RUL.

A piece-wise linear degradation model is used for the true RUL, allowing for a constant RUL phase at the beginning first three days to limit under-estimating and to factor in a degree of usage prior to degradation (noting this is factored into the numerical case at under 5%). The RUL estimation at mid-life and approaching failure threshold performs well, and this is reflected in the RMSE value of 7.05 samples and score function result of 17.38, which is consistent with other PHM model results and greatly improved, as is to be expected for a numerical case [3]. If the RMSE is taken for the beginning and end-

of-life stages (first 15 samples and last 15 samples), where typically the end-of-life stage is most critical for operations and maintenance planning, the RMSE is 9.72 and 1.31 samples, respectively. The relatively high beginning-of-life RMSE value is expected as the model confidence interval is large; however, as more test points update the model, the RMSE greatly reduces, with the accuracy of the predicted RUL increasing to a probability of 90%. This, for example, could enable maintainers to make a proactive decision on rectifying the free-play well in advance of the nominal threshold and perform or plan maintenance more effectively, or ready the supply chain for part replacement.

CONCLUSION

In summary, this paper contributes a numerical benchmark case for aircraft control surface free-play degradation and outlines a PHM approach for the estimation of RUL. Signal processing of the TE wing tip displacements is performed in the time- and frequency-domains, generating signal features (e.g., peak frequency, peak amplitude, etc.). Monotonic analysis of the signal response features enables training of the prognostics exponential degradation model. The novelty is in the development of a numerical case capable of generating synthetic free-play degradation data from dynamic flight profiles. Furthermore, the exponential prognostics approach performs well using TE wing tip responses at some spatial distance from the free-play source. Future work will focus on: i) refining the free-play degradation model, including more growth factors; ii) developing a numerical case of a GFA empennage control surfaces (e.g., all-movable stabilator) with actuator free-play and increased spatial distance from free-play source to sensor (e.g., low fidelity strain responses); and iii) more realistic flight conditions that includes high angle-of-attack manoeuvres that encounter vortex buffet loading. A related focus of the research is to enhance the prognostics model for more robust RUL estimation and to later apply this approach to a larger surrogate dataset of actual aircraft on-board sensor responses.

ACKNOWLEDGEMENTS

The authors are grateful for the ongoing research collaboration with the Australian Defence Science and Technology Group (DSTG) and the domain knowledge that the subject matter experts bring to projects. This research was supported by the Defence Science Institute, an initiative of the State Government of Victoria, under Research Higher Degree (RHD) Student Grant number 35761.

REFERENCES

[1] (1990) “MIL-STD-1797A Flying Qualities of Piloted Aircraft.” US Department of Defense Interface Standard.

[2] P. C. Chen and D. H. Lee, (2008) “Flight-Loads Effects on Horizontal Tail Free-Play-Induced Limit Cycle Oscillation,” *J. Aircr.*, vol. 45, no. 2, pp. 478–485, doi: 10.2514/1.29611.

[3] M. J. Scott, W. J. C. Verhagen, O. Levinski, and P. Marzocca, (2023) “A Structural PHM Framework for Aircraft Control Surface Free-play,” in *AIAC20: 20th Australian International Aerospace Congress*, Melbourne, Australia: Engineers Australia, Royal Aeronautical Society.

[4] S. C. Jensen, G. D. Jenney, and D. Dawson, (2000) “Flight test experience with an electromechanical actuator on the F-18 Systems Research Aircraft,” in *19th DASC. 19th Digital Avionics Systems Conference. Proceedings (Cat. No.00CH37126)*, p. 2E3/1-2E310 vol.1. doi: 10.1109/DASC.2000.886914.

[5] J. Newcamp, W. J. C. Verhagen, and R. Curran, (2016) “Correlation of mission type to cyclic loading as a basis for agile military aircraft asset management,” *Aerosp. Sci. Technol.*, vol. 55, pp. 111–119, doi: 10.1016/j.ast.2016.05.022.

[6] G. Di Rito, F. Schettini, and R. Galatolo, (2018) “Model-Based Prognostic Health-Management Algorithms for the Freeplay Identification in Electromechanical Flight Control Actuators,” in *2018 5th IEEE International Workshop on Metrology for AeroSpace (MetroAeroSpace)*, pp. 340–345. doi: 10.1109/MetroAeroSpace.2018.8453552.

[7] L. Baldo, I. Querques, M. D. L. Dalla Vedova, and P. Maggiore, (2023) "A Model-Based Prognostic Framework for Electromechanical Actuators Based on Metaheuristic Algorithms," *Aerospace*, vol. 10, no. 3, Art. no. 3, doi: 10.3390/aerospace10030293.
[8] A. C. Bertolino, A. De Martin, G. Jacazio, and M. Sorli, (2023) "Design and Preliminary Performance Assessment of a PHM System for Electromechanical Flight Control Actuators," *Aerospace*, vol. 10, no. 4, Art. no. 4, doi: 10.3390/aerospace10040335.
[9] M. Candon, O. Levinski, H. Ogawa, R. Carrese, and P. Marzocca, (2022) "A nonlinear signal processing framework for rapid identification and diagnosis of structural freeplay," *Mech. Syst. Signal Process.*, vol. 163, p. 107999, doi: https://doi.org/10.1016/j.ymssp.2021.107999.
[10] M. Scott, A. Das, M. Candon, W. J. Verhagen, O. Levinski, and P. Marzocca, (2023) "A Data-Driven Approach to Control Surface Free-play Diagnostics with Actuator Load Responses," in *AIAA SCITECH 2023 Forum*, in AIAA SciTech Forum. American Institute of Aeronautics and Astronautics. doi: 10.2514/6.2023-2219.
[11] M. J. Candon, M. Scott, S. Koschel, O. Levinski, and P. Marzocca, (2021) "A Data-Driven Signal Processing Framework for Enhanced Freeplay Diagnostics in NextGen Structural Health Monitoring Systems," in *AIAA SCITECH 2022 Forum*, in AIAA SciTech Forum. American Institute of Aeronautics and Astronautics. doi: 10.2514/6.2022-2131.
[12] M. J. Scott, W. J. C. Verhagen, M. T. Bieber, and P. Marzocca, (2022) "A Systematic Literature Review of Predictive Maintenance for Defence Fixed-Wing Aircraft Sustainment and Operations," *Sensors*, vol. 22, no. 18, p. 7070, doi: 10.3390/s22187070.
[13] E. C. Yates Jr, (1988) "AGARD Standard Aeroelastic Configurations for Dynamic Response I - Wing 445.6," AGARD, Oberammergau, Germany, Paper presented at the 61st Meeting of the Structures and Materials Panel, 8-13 September 1985 AGARD Report No.765. Accessed: Sep. 27, 2022. [Online]. Available: https://apps.dtic.mil/sti/citations/ADA199433
[14] W. A. Silva, P. Chwalowski, and B. Perry, (2014) "Evaluation of linear, inviscid, viscous, and reduced-order modelling aeroelastic solutions of the AGARD 445.6 wing using root locus analysis," *Int. J. Comput. Fluid Dyn.*, vol. 28, no. 3–4, pp. 122–139, doi: 10.1080/10618562.2014.922179.
[15] R. Carrese, N. Joseph, P. Marzocca, and O. Levinski, (2017) "Aeroelastic Response of the AGARD 445.6 Wing with Freeplay Nonlinearity," in *58th AIAA/ASCE/AHS/ASC Structures, Structural Dynamics, and Materials Conference*, Grapevine, Texas: American Institute of Aeronautics and Astronautics. doi: 10.2514/6.2017-0416.
[16] M. Karpel and D. Raveh, (1996) "Fictitious mass element in structural dynamics," *AIAA J.*, vol. 34, no. 3, pp. 607–613, doi: 10.2514/3.13111.
[17] (1993) "MIL-A-8870C, Military Specification: Airplane Strength And Rigidity Vibration, Flutter, And Divergence." Accessed: Oct. 03, 2021. [Online]. Available: http://everyspec.com/MIL-SPECS/MIL-SPECS-MIL-A/MIL-A-8870C_6746/
[18] P. L. Swagel, (2022) "Availability and Use of F-35 Fighter Aircraft | Congressional Budget Office," Congressional Budget Office. Accessed: Apr. 04, 2023. [Online]. Available: https://www.cbo.gov/publication/57966
[19] (2019) "Pilatus PC-9/A Maintenance Manual." Pilatus Aircraft Ltd.
[20] V. Goblet, N. Fala, and K. Marais, (2015) "Identifying Phases of Flight in General Aviation Operations," doi: 10.2514/6.2015-2851.
[21] V. Singh, (2017) "Fuel consumption minimization of transport aircraft using real-coded genetic algorithm," *Proc. Inst. Mech. Eng. Part G J. Aerosp. Eng.*, vol. 232, p. 095441001770589, doi: 10.1177/0954410017705899.
[22] O. Gallego, R. Perez, and P. Jansen, (2018) "Technical Viability and Operational Assessment of a Supersonic Business Jet," doi: 10.2514/6.2018-3661.
[23] G. E. Cooper and R. P. Harper, (1969) "The Use Of Pilot Rating In The Evaluation Of Aircraft Handling Qualities," National Aeronautics and Space Administration (NASA), Washington, D.C., NASA Technical Note NASA-TN-D-5153. Accessed: Apr. 23, 2023. [Online]. Available: https://ntrs.nasa.gov/citations/19690013177
[24] E. Martin, (2023) "Boeing Statistical Summary Of Commercial Jet Airplane Accidents Worldwide Operations | 1959 – 2021."

[25] M. H. Sadraey, (2017) *Aircraft Performance: An Engineering Approach*. Boca Raton: CRC Press. doi: 10.1201/9781315366913.
[26] J. Panchal and H. Benaroya, (2021) "Review of control surface freeplay," *Prog. Aerosp. Sci.*, p. 100729, doi: 10.1016/j.paerosci.2021.100729.
[27] "Exponential degradation model for estimating remaining useful life - MATLAB - MathWorks Australia." Accessed: Oct. 10, 2022. [Online]. Available: https://au.mathworks.com/help/predmaint/ref/exponentialdegradationmodel.html
[28] N. Borst and W. J. Verhagen, (2021) "Improving Remaining Useful Life Prediction of Complex Systems through CNN-LSTM Network Adaptations," in *AIAC 2021: 19th Australian International Aerospace Congress*, Melbourne, Australia: Engineers Australia, pp. 92–97. doi: 10.3316/informit.313549972769307.
[29] Y. Zhou, Y. Gao, Y. Huang, M. Hefenbrock, T. Riedel, and M. Beigl, (2020) "Automatic Remaining Useful Life Estimation Framework with Embedded Convolutional LSTM as the Backbone." arXiv. Accessed: Oct. 18, 2022. [Online]. Available: http://arxiv.org/abs/2008.03961
[30] P. Lim, C. K. Goh, K. C. Tan, and P. Dutta, (2014) "Estimation of Remaining Useful Life Based on Switching Kalman Filter Neural Network Ensemble," *Annu. Conf. Progn. Health Manag. Soc. 2014*, p. 8.
[31] A. Saxena *et al.*, (2008) "Metrics for evaluating performance of prognostic techniques," in *2008 International Conference on Prognostics and Health Management*, Denver, CO, USA: IEEE, pp. 1–17. doi: 10.1109/PHM.2008.4711436.